Published in final edited form as:
Circ Arrhythm Electrophysiol. 2012 February 1; 5(1): 181–190. doi:10.1161/CIRCEP.111.967265.

Spontaneous Ventricular Fibrillation in Right Ventricular Failure Secondary to Chronic Pulmonary Hypertension

Soban Umar, MD, PhD[1,4], **Jong-Hwan Lee, MD, PhD**[2,4,5], **Enno de Lange, PhD**[2,4], **Andrea Iorga, BSc**[1,4], **Rod Partow-Navid, BSc**[1,4], **Aneesh Bapat, BSc**[2,4], **Arnoud van der Laarse, PhD**[6], **Rajeev Saggar, MD**[2,3], **Rajan Saggar, MD**[2,3], **Dirk L. Ypey, PhD**[6], **Hrayr S. Karagueuzian, PhD, FACC**[2,4], and **Mansoureh Eghbali, PhD**[1,4]

[1]Dept of Anesthesiology, David Geffen School of Medicine at UCLA, Los Angeles, CA [2]Dept of Medicine, David Geffen School of Medicine at UCLA, Los Angeles, CA [3]Division of Pulmonary & Critical Care Medicine, David Geffen School of Medicine at UCLA, Los Angeles, CA [4]Cardiovascular Research Laboratories, David Geffen School of Medicine at UCLA, Los Angeles, CA [5]Department of Anesthesiology & Pain Medicine, Samsung Medical Center, Sungkyunkwan University School of Medicine, Seoul, Korea [6]Department of Cardiology, Leiden University Medical Center, Leiden, the Netherlands

Abstract

Background—Right ventricular failure (RVF) in pulmonary hypertension (PH) is associated with increased incidence of sudden death by a poorly explored mechanism. Here we test the hypothesis that PH promotes spontaneous ventricular fibrillation (VF) during a critical post-PH onset period characterized by a sudden increase in mortality.

Methods and Results—Rats received either a single subcutaneous dose of monocrotaline (MCT, 60 mg/kg) to induce PH-associated RVF (PH, n=24) or saline (CTRL, n=17). Activation pattern of RV-epicardial surface was mapped using voltage-sensitive dye in isolated Langendorff-perfused hearts along with single glass-microelectrode and ECG-recordings. MCT-injected rats developed severe PH by day-21 and progressed to RVF by ~day-30. Rats manifested increased mortality and ~30% rats died suddenly and precipitously during 23–32 days post-MCT. This fatal period was associated with the initiation of spontaneous VF by a focal mechanism in the RV which was subsequently maintained by both focal and incomplete re-entrant wavefronts. Microelectrode recordings from the RV-epicardium at the onset of focal activity showed early afterdepolarization (EAD)-mediated triggered activity that led to VF. The onset of the RV cellular triggered beats preceded left ventricular depolarizations by 23±8 ms. The RV but not the LV cardiomyocytes isolated during this fatal period manifested significant action potential duration prolongation, dispersion and an increased susceptibility to depolarization-induced repetitive activity. No spontaneous VF was observed in any of the CTRL hearts. RVF was associated with significantly reduced RV ejection fraction ($p<0.001$), RV hypertrophy ($p<0.001$) and RV fibrosis ($p<0.01$). The hemodynamic function of the LV and its structure were preserved.

Conclusions—PH-induced RVF is associated with a distinct phase of increased mortality characterized by spontaneous VF arising from the RV by an EAD-mediated triggered activity.

Correspondence: Mansoureh Eghbali, PhD, Dept. of Anesthesiology, UCLA School of Medicine, BH-160CHS, 650 Charles Young Dr., Los Angeles, CA 90095-7115, Tel: (310) 206-0345, Fax: (310) 825-6649, meghbali@ucla.edu.

Conflict of Interest Disclosures: None

Keywords

pulmonary hypertension; right ventricular failure; early afterdepolarization; optical mapping; ventricular fibrillation

Introduction

Pulmonary hypertension (PH) is a lethal syndrome caused by arteriolar obstruction resulting from excessive proliferation of pulmonary artery smooth muscle and endothelial cells, endothelial dysfunction, inflammation, and excessive vasoconstriction [1, 2]. Long-standing pressure-overload in PH leads to right ventricular (RV) hypertrophy and subsequently diastolic and systolic RV failure (RVF)[3, 4]. In fact, RVF is the most common cause of death in PH patients (~30–50% of deaths). Sudden death has also been reported to account for ~17–28% of deaths in these patients [5, 6]. While pulmonary vascular disease has been the primary pathologic focus, less attention has been paid to the potential of direct lethal arrhythmic consequences of the RV as a cause of sudden death in PH. For example, the electrical[7] and structural[8] remodelling of the RV associated with PH could potentially provide both substrate and trigger for the initiation of spontaneous ventricular fibrillation (VF), a major cause of sudden cardiac death[9]. Ample experimental studies in rats have shown that a single injection of the toxic alkaloid monocrotaline (MCT) successfully recapitulates the major pulmonary arterial and RV pathological features of PH in man including the sudden and precipitous rise in mortality [7, 8, 10]. Furthermore, changes in ventricular gradient and QT interval were also seen both in PH patients[11, 12] and in animal models of PH[3, 13, 14]. MCT-induced PH is found to also prolong the RV action potential duration[3, 7, 15] in association with downregulation of K^+ channels [3, 7, 14]. However, to our knowledge a combined systematic intact heart and cellular electrophysiological, hemodynamic and histo-biochemical study of the RV and the left ventricle (LV) and their respective roles in the initiation of spontaneous VF in chronic PH is still lacking. The purpose of this study was to test the hypothesis that chronic PH promoted spontaneous VF during a critical post-PH period is associated with major structural and electrophysiological remodelling of the RV but not the LV providing both the substrate and the trigger for spontaneous VF.

Methods

Animals, treatment and mortality criteria

Chronic PH-associated RVF was induced in male Sprague-Dawley rats (3–4 months, 350–400 g) by a single s.c. injection of 60 mg/kg monocrotaline (MCT, n=24) and compared to saline-treated control rats (CTRL, n=17). Details of the treatment and criteria for mortality are given in the online data supplement.

Cardiac and pulmonary hemodynamics

Serial B-Mode, M-Mode and pulmonary pulsed-wave Doppler echocardiography were performed using a VisualSonics Vevo 770 (VisualSonics, Ontario, Canada) equipped with a 30-MHzlinear transducer to accurately monitor cardiopulmonary hemodynamics as described in details in the supplement. RV and LV pressures were measured by direct cardiac catheterization at the end of the 4^{th} week prior to sacrifice.

Whole heart isolated-perfused Langendorff studies and optical mapping

After excision of the heart, the ascending aorta was cannulated for retrograde perfusion with warm (36.5±0.5°C) oxygenated Tyrode solution and mounted in a tissue bath for optical

mapping of RV activation patterns as we previously described [16]. The hearts were stained with the voltage–sensitive dye, RH237 (Invitrogen Molecular Probes, Carlsbad, CA) for fluorescent optical mapping of the RV epicardial surface. Cytochalasin D (5 μmol/L) was added to the perfusate to inhibit motion. Single cell action potentials were recorded with glass microelectrode from selected RV epicardial surface areas that optical mapping showed focal activity in order to determine the cellular mechanisms of the focal activity. An epicardial wavefront was considered to be focal when it arose from within the RV mapped region (i.e., did not propagate into the mapped region from the outside) and was surrounded by recovered tissue [16]. A total of 9 hearts were studied (n=5 for CTRL, and n=4 for PH).

Isolated cardiomyocytes studies and immunocytochemistry imaging

At the end of the 4th week, the hearts were dissociated with collagenase. RV and LV cardiomyocytes were isolated as described before [8] and in the online supplement. A total of 10 hearts were used (n=5/group). Freshly isolated myocytes were fixed and stained with antibodies. Images were acquired with a high-resolution confocal microscope.

Whole-cell patch-clamp experiments

Membrane potentials of RV-cardiomyocytes (n=5/group) were measured with the patch-clamp technique in the whole-cell current-clamp configuration. The details of patch-clamp experiments are described in the online supplement.

Gross histological evaluation

The RV-wall, the LV-wall and the interventricular septum (IVS) were dissected, weighed, and the weight ratio of RV/(LV+IVS) was calculated as an index of RV-hypertrophy. The LV/body weight ratio was used as an index for LV-hypertrophy.

Real Time PCR and Western blot analysis

Standard real-time PCR and Western blot were performed. The details of procedures are described in the online data supplement.

Immunohistochemistry and imaging

Hearts were fixed and transversal 6–7 μm sections were obtained. Tissue sections were stained with immunofluorescence, standard hematoxylin/eosin and Masson trichrome stain (see online data supplement for details).

Statistical analysis

Means were compared between the control and PH groups using t tests as all outcomes were well modelled by Gaussian (normal) distribution. A two-sided *P* value less than 0.05 was considered statistically significant. Means and standard errors of the mean (SEMs) are reported.

Results

Effects of chronic PH on mortality, cardiac hemodynamics and cardiac structure

Severe PH was evident ~4 weeks after MCT injection by the presence of mid-systolic notching on pulmonary artery flow profile in pulsed wave Doppler echocardiography (Fig. 1A). Direct RV catheterization confirmed the severity of PH as the RV peak systolic pressure (RVPSP) was 2.5-fold higher in the PH group than in the controls (Table. 1). LV pressures remained unchanged ~4 weeks after MCT treatment (Table. 1). MCT-induced PH selectively depressed the function of the RV as demonstrated by the decrease of the RV

ejection fraction (RVEF) from 72% at day 14 to 38% at day 21 (Fig. 1C). Thereafter and up to the time of the sacrifice, the RVEF of the MCT-treated rats remained in the range of 30–35%. In contrast to RV, the LV function was fully preserved with no change in the LVEF for the entire 30 days post-MCT period (Table. 1). Sudden unexpected deaths in the PH group occurred from day 23 onwards (~30%), and all rats died by day 32 post-MCT treatment (Fig. 1C). We defined the period between days 23–32 as the "sudden death period". It is of interest to note that the precipitous drop in the RVEF from days 14 to 21 preceded by about 10 days the precipitous rise in the incidence of sudden deaths in the MCT-treated rats. The lack of temporal correlation between the RV hemodynamic worsening and the emergence of spontaneous VF suggests that it is the electrical failure rather than the hemodynamic deterioration as the primary inciting factor for the VF (Fig. 1C). MCT-induced PH caused major structural changes in the RV but not in LV. The RV changes included hypertrophy as reflected by the increased ratio of RV/(LV+IVS) weights and an increase in the RV cardiomyocyte size (Table. 1 and Fig. 2A,B). A significant increase in RV fibrosis both in the epicardium (17±2% *vs.* 1.5±0.4% in CTRL) and in the endocardium (18±3% *vs.* 1.4±0.3% in CTRL (Fig. 2C) was evident in the MCT-induced PH group. In addition, the expression levels of the pro-apoptotic cleaved caspase-3 protein were significantly increased in the RV reflecting the presence of apoptosis/necrosis in the failing RV (Fig. 2D). In contrast to RV, the structure of the LV was preserved, as there were no signs of hypertrophy, fibrosis or apoptosis.

Spontaneous initiation of VF in chronic PH rat hearts

In order to gain insight into the cellular mechanism of spontaneous VF initiation, we continuously monitored the ECG, LV and LA bipolar electrograms and single cell action potentials recorded with microelectrode from the base of the RV epicardium of the isolated RV failed hearts during the sudden death period (i.e., days 23 to 32 post-MCT). We successfully captured six spontaneous initiations of VF episodes in four hearts during continuous electrical recordings. Figure 3 illustrates one example of spontaneous VF that emerged in an isolated heart 29 days after MCT treatment. The onset of VF was preceded by EADs, followed by EAD-mediated triggered single beat (Fig. 3A), which then evolved to EAD-mediated triggered activity causing non-sustained VT (Fig. 3B) which on subsequent triggered episode degenerated to VF (Fig. 3C). The upstroke of the RV cellular EAD-mediated triggered activity recorded with the microelectrodes preceded the onset of the LV bipolar electrogram and the QRS of the pseudo-ECG by 14±6 ms and 28±8 ms respectively (6 episodes, 4 hearts) (Figure 3). This indicates that the triggered activity arising from the RV drives the LV. The VFs were terminated by electrical shocks and several minutes later another episode of spontaneous VF reemerged. In control saline-treated rat hearts no VF emerged for up to 3 hours of perfusion with normal Tyrode's (n=5).

In order to determine whether the RV epicardial surface of the MCT-treated hearts manifests conduction block that might result from an anatomical obstacle in the failing and structurally remodeled fibrotic RV, we optically mapped the RV epicardial surface using voltage–sensitive dye RH-237. As shown in Fig. 4A, no conduction block developed over the epicardial surface of the failed RV during either pacing or during normal sinus rhythm indicating the absence of anatomic obstacles over the epicardial surface of the failed RV. In order to determine the mechanism(s) by which the VF in the failing RV is maintained once initiated by an EAD-mediated triggered activity; we optically mapped the RV epicardial surface in three MCT-treated hearts 10 sec after the onset of VF. Both focal and incomplete reentrant wavefronts were observed during all six episodes of VF in all four hearts (Fig 5 and Supplemental Fig. 2). As shown in Fig. 5 activation map during the VF showed two competing foci (labelled 1 & 2 in Fig 5B). While both foci had a frequency of 14 HZ, the focus originating from site 1 activated the surrounding RV myocardium with a 2:1 pattern

causing the surrounding portion of the RV to be activated at a frequency of 7 Hz (Fig 5C). The optical action potentials (OAPs) recorded from the two foci and the RV surrounding site with a 2:1 block are shown in Fig 5D. Focal activity was defined as an island of depolarized tissue on the epicardial surface surrounded by recovered tissue.

Mechanisms of increased susceptibility of PH hearts to EADs and triggered activity

Theoretical and experimental studies have shown that reduced repolarization reserve, increased myocardial fibrosis and elevated cytosolic Ca levels promote EADs and triggered activity that could lead to VF [16–21]. Cardiomyocytes isolated from failing RV, unlike cardiomyocytes isolated from the LV, had their APD90 (90 percent repolarization) prolonged from 33±6 ms (control) to 57±8 ms in the MCT-treated hearts ($p<0.001$) (Fig. 6A) suggesting reduced repolarization reserve, a major characteristic of failing cardiomyocytes [22]. Furthermore, cells isolated from the RV of MCT-treated hearts manifested significantly greater dispersion in APD90 (maximum APD minus minimum APD) compared to control (30±1.8 ms vs. 20±1.5 ms, 16 cells in 5 hearts, $p<0.01$). Since the potential of depolarizing influences exerted by fibroblasts in hearts with increased fibrosis could promote EADs and triggered activity [17, 18, 21], we tested the influence of long duration (1.6 s) depolarizing current pulses on depolarization induced triggered activity (TA) in isolated control and failing RV cardiomyocytes. Unlike the LV cardiomyocytes, RV cardiomyocytes isolated from MCT-treated hearts manifested TA with higher frequency (Fig. 6B) and higher amplitudes than control RV cardiomyocytes in response to a given depolarizing current pulse (4.2±0.37 vs. 2.5±0.28 action potentials per 1.6 s pulse, $p<0.01$, and 65.2±4.7 mV vs. 45±3.5 mV measured at the end of the 1.6 s period, $p<0.05$, respectively).

Electrophysiological changes seen in PH myocytes could not be attributed to direct effects of MCT as bath application of MCT had no effect on action potential configuration in isolated RV and LV myocytes[7] (Supplemental Fig. 3).

In summary, our findings indicate that the cardiomyocytes from PH group with reduced repolarization reserve manifest greater susceptibility to generate triggered activity that could lead to VT and VF.

To determine the possible molecular mechanisms associated with reduced repolarization reserve, we examined the expression of sarcoplasmic reticulum calcium-sensitive ATPase (SERCA2a) as well as the molecular correlates of the major repolarizing currents in rodents, i.e., IK_{Slow}, Kv1.5 and Kv2.1, in the RV and LV of PH rats during the sudden cardiac death period (i.e., 23–32 post-MCT treatment days). PH caused a selective and a considerable reduction (by 94%) in the level of SERCA2a protein in the RV of PH group (0.06±0.01) vs. control (1.00±0.26, $p<0.05$) (Supplemental Fig. 1) without affecting SERCA2a level in the LV. Real time PCR revealed that Kv1.5 transcripts, but not Kv2.1, were downregulated by 50% in the RV of PH hearts (Fig. 7A). Consistent with the lower Kv1.5 transcript levels in PH group, Kv1.5 protein levels in RV were also downregulated by 88% (from 1.00±0.18 to 0.12±0.03, $p<0.05$) but not in the LV (Fig. 7B). Kv1.5 immunoreactivity was also lower in RV cardiomyocytes in PH group but not in the LV cardiomyocytes (Fig. 7C). KCNE2, an ancillary K^+ channel subunit, has been shown to physically associate with Kv1.5 in murine heart [23] and its ablation has been shown to result in 50% reduction of IK_{slow} leading to APD prolongation [23]. KCNE2 protein expression was ~4-fold lower in the PH group than in the controls ($p<0.05$) in RV (Fig. 7D) with total absence in the T-tubules being confined only to the cell surface membrane in RV cardiomyocytes (Fig. 7E). There was no change in KCNE2 protein or immunolocalization in the LV.

Discussion

Major findings

Spontaneous VF initiated by EAD-mediated triggered activity in hearts with PH-induced RV electrophysiological, hemodynamic and structural remodelling constitutes the major finding of this study. This study also highlights that the structure and the function of the LV, unlike the RV, remain fully preserved during the course of the chronic PH.

Selective RV remodelling secondary to chronic PH

Here we show selective functional, structural and electrical remodelling only in the RV, but not in the LV of PH group consistent with previous reports [24–26]. However, relatively minor LV remodeling has also been reported in chronic PH. For example, Lamberts et al. have shown structural changes in the LV resulting in a moderately depressed LV diastolic function along with minor increase in LV fibrosis[27]. Benoist et al[28] using the MCT model of PH in rats, found that the remodelled RV had a steeper slope of monophasic APD restitution curve than the LV causing increased susceptibility to rapid pacing-induced VF in these remodeled hearts. Furthermore, these authors found that the prolongation of the APD was considerably more in the RV compared to LV (90% vs. 15%)[28].

Mechanism of spontaneous VF

Single cell microelectrode recording from the RV epicardial surface near the base showed that the spontaneous VF was initiated by EAD-mediated triggered activity causing VT, which then degenerates to VF (Fig. 3,5). Importantly the emergence of EADs on the RV epicardial surface coincided in time with the isoelectric interval of the simultaneously recorded LV and pseudo-ECG (Fig. 3A) and preceded the activation of the LV indicating that the failed RV was driving the LV during the EAD-mediated triggered activity. This finding suggests that the RV is the site of origin of the trigger for VF in rats with severe PH induced by MCT. In addition, the increased dispersion of repolarization observed in the failing RV cardiomyocytes could promote reentry that may contribute to the maintenance of VF. In fact our optical activation mapping of the RV epicardial surface using epifluorescent voltage-sensitive dye showed that the spontaneous VF is maintained by both focal and incomplete re-entrant mechanisms.

It may be argued that the increased incidence of deaths may directly result from the severe RV hemodynamic deterioration associated with chronic PH. However, the differential time-course of RV hemodynamic deterioration and increased mortality argues for RV electrical dysfunction rather than the depressed hemodynamic function of the RV as a primary cause of death in our rat model of MCT-induced PH. Indeed the RV function deteriorated precipitously between days 14 and 21 as the RVEF fell steeply from ~72% at day 14 to ~38% at day 21 at a time period when most of the PH rats were still alive. The highest incidence of sudden and precipitous deaths occurred between days 23–32, some 10 days *after* the maximum attainable decrease in RVEF (Fig. 1C). These findings suggest that the mortality during the sudden death period is caused by EAD-mediated triggered activity in the RV. However, we cannot exclude the potential role of severe RV hemodynamic depression in the initiation of spontaneous VF *in vivo*. It is possible that the depressed RVEF may conspire with electrical remodelling to promote VF *in vivo*. A recent report showed increased susceptibility to electrically inducible arrhythmias in rat hearts with MCT-induced PH however, no spontaneous VF, was documented in this study [28].

Molecular and structural determinants of EAD-mediated triggered activity

While EADs are readily induced in isolated ventricular cardiomyocytes [18, 19], however, EADs at the tissue level may be suppressed by source-to-sink mismatches arising from cell-

to-cell coupling [17–19]. That is, a small current which is sufficient to reverse repolarization and cause an EAD in an isolated cardiomyocyte will be diluted into adjacent repolarizing cardiomyocytes (unless they are also simultaneously primed for an EAD), thereby suppressing the EAD [17, 18]. The increased RV fibrosis observed in the MCT-treated hearts promotes partial cellular uncoupling by interstitial collagen deposition that effectively reduces that sink effect, thereby allowing susceptible cardiomyocytes in the RV to generate EADs and triggered activity causing VF [16–19].

In addition to increased fibrosis in the RV, relatively selective reduction of RV myocyte repolarization reserve could also facilitate the formation of EADs. In this respect, selective downregulation of Kv1.5 in RV but not LV as shown here and in previous studies [3, 7], may contribute to the enhanced susceptibility of the RV myocytes to generate EADs in the PH group. Furthermore selective downregulation of KCNE2, an ancillary K^+ channel subunit, and its disappearance from t-tublues in the RV but not the LV in the MCT-treated rats may contribute to RV arrhythmogenesis as inherited mutations in this gene are associated with human cardiac arrhythmogenesis.[29] Disappearance of KCNE2 from the T-tubules during sudden cardiac death period further disrupts its association with Kv1.5 that may result in further reduction of repolarization reserve. The reduced repolarization reserve of the failing RV cardiomyocytes was associated with increased frequency and increased amplitude of depolarization-induced triggered activity further supporting the mechanism of cellular EAD-mediated triggered activity recorded in the whole heart. Selective downregulation of SERCA2a protein in failing RV cardiomyocytes as shown here and by others [26] is expected to slow Ca^{2+} ion uptake by the sarcoplasmic reticulum [30] after each beat causing an elevation of intracellular Ca^{2+} concentration. This phenomenon is known to activate the forward mode for the Na^+-Ca^{2+} exchanger providing a net inward current that further reduces repolarization reserve and facilitates EAD formation in the failing RV cardiomyocytes [31, 32]. In addition to SERCA2a, Kogler et al., found that other calcium-handling proteins such as phospholamban and ryanodine receptor were also downregulated only in the RV, but not in the LV of MCT-treated rats[26]. In a recent study Miura et al. suggested that an increase in diastolic $[Ca^{2+}]i$ and an increase in Ca^{2+} sensitivity of the sarcoplasmic reticulum Ca^{2+} release channel accelerate Ca^{2+} waves in ventricular hypertrophy, thereby causing arrhythmogenesis in the RV of MCT-induced PH[33].

Limitations

In epicardial surface maps, an intramural wave front breaking through the surface may have the appearance of a focal activation. The fibrotic and apoptotic/necrotic changes in the endocardium of the RV may limit breakthroughs suggesting an intrinsic role of the epicardial cells in the genesis of triggered foci. In our previous study [16] we have shown that the destruction of the endocardial Purkinje network by cryoablation did not prevent epicardial muscle cells to generate EADs suggesting an intrinsic ability of epicardial cardiomyocytes to generate EAD-mediated triggered activity. In line with this argument is the presence of EADs by epicardial cardiomyocytes of failing RV that occur during the isoelectric interval on the pseudo-ECG and more importantly precede the activation of the LV indicate the absence of electrical activity elsewhere in the heart during epicardial EAD formation and that the failing RV drives the LV during the EAD-mediated triggered activity.

Clinical implications

The mechanism of increased premature mortality in RV-failure associated with chronic PH is still unresolved [34]. Chronic PH is associated with increased incidence of sudden cardiac death [9] by mechanisms that are not fully understood. Here we report that VF can be a potential mechanism of sudden premature death during chronic PH induced by MCT, a model of experimental PH which recapitulates the major features of RV-hypertrophy and

RV-failure in man [8, 10, 35]. However, we cannot exclude the potential role of depressed contractile RV-function and RV ischemia[36] that could conspire with the electrical remodelling to facilitate the emergence of EAD-mediated VT and VF.

Although idiopathic PAH is perceived as a progressive disease with uniformly poor outcome, the natural history of the disease is heterogeneous, with some patients dying within months and others living for decades[37]. Despite the advances in vasodilator/vasomodulating therapies altering the course of the disease, still the most common causes of death remain RV-failure and sudden death[6]. To the extent that our findings in the MCT-rat model would bear resemblance to human PH-induced RV failure spontaneous VF may be considered a potential mechanism of death in this dreadful syndrome. However, more clinical work is needed in patients with severe PH to determine the incidence of spontaneous VF as a cause of premature death in these patients.

Conclusions

Chronic PH is associated with selective electrophysiological, hemodynamic and structural remodelling of the RV, but not the LV. Selective RV downregulation of (i) the molecular correlates of IK_{Slow} expression Kv1.5 and KCNE2, (ii) downregulation of SERCA2a, (iii) increased RV fibrosis, (iv) increased RV apoptosis/necrosis promote EAD-mediated triggered activity in the RV leading to VF during a critical post-PH vulnerable period of RV-failure. This mechanism combined with severe RV hemodynamic compromise may conspire to account for the high rate of sudden deaths in patients with chronic PH [35, 38].

Supplementary Material

Refer to Web version on PubMed Central for supplementary material.

Acknowledgments

Funding Sources: NIH-grants HL089876 and HL089876S1 (M.E).

References

1. Farber HW, Loscalzo J. Pulmonary arterial hypertension. N Engl J Med. 2004; 351:1655–1665. [PubMed: 15483284]
2. Abe K, Toba M, Alzoubi A, Ito M, Fagan KA, Cool CD, Voelkel NF, McMurtry IF, Oka M. Formation of plexiform lesions in experimental severe pulmonary arterial hypertension. Circulation. 2010; 121:2747–2754. [PubMed: 20547927]
3. Piao L, Fang YH, Cadete VJ, Wietholt C, Urboniene D, Toth PT, Marsboom G, Zhang HJ, Haber I, Rehman J, Lopaschuk GD, Archer SL. The inhibition of pyruvate dehydrogenase kinase improves impaired cardiac function and electrical remodeling in two models of right ventricular hypertrophy: resuscitating the hibernating right ventricle. J Mol Med. 2010; 88:47–60. [PubMed: 19949938]
4. Gan CT, Holverda S, Marcus JT, Paulus WJ, Marques KM, Bronzwaer JG, Twisk JW, Boonstra A, Postmus PE, Vonk-Noordegraaf A. Right ventricular diastolic dysfunction and the acute effects of sildenafil in pulmonary hypertension patients. Chest. 2007; 132:11–17. [PubMed: 17625080]
5. Hoeper MM, Galie N, Murali S, Olschewski H, Rubenfire M, Robbins IM, Farber HW, McLaughlin V, Shapiro S, Pepke-Zaba J, Winkler J, Ewert R, Opitz C, Westerkamp V, Vachiery JL, Torbicki A, Behr J, Barst RJ. Outcome after cardiopulmonary resuscitation in patients with pulmonary arterial hypertension. Am J Respir Crit Care Med. 2002; 165:341–344. [PubMed: 11818318]
6. Humbert M, Sitbon O, Chaouat A, Bertocchi M, Habib G, Gressin V, Yaici A, Weitzenblum E, Cordier JF, Chabot F, Dromer C, Pison C, Reynaud-Gaubert M, Haloun A, Laurent M, Hachulla E, Cottin V, Degano B, Jais X, Montani D, Souza R, Simonneau G. Survival in patients with idiopathic, familial, and anorexigen-associated pulmonary arterial hypertension in the modern management era. Circulation. 2010; 122:156–163. [PubMed: 20585011]

7. Lee JK, Kodama I, Honjo H, Anno T, Kamiya K, Toyama J. Stage-dependent changes in membrane currents in rats with monocrotaline-induced right ventricular hypertrophy. Am J Physiol. 1997; 272:H2833–H2842. [PubMed: 9227563]
8. Umar S, de Visser YP, Steendijk P, Schutte CI, Laghmani EH, Wagenaar GTM, Bax WH, Mantikou E, Pijnappels DA, Atsma DE, Schalij MJ, van der Wall EE, van der Laarse A. Allogenic stem cell therapy improves right ventricular function by improving lung pathology in rats with pulmonary hypertension. Am J Physiol Heart Circ Physiol. 2009; 297:H1606–H1616. [PubMed: 19783775]
9. Zipes DP, Wellens HJ. Sudden cardiac death. Circulation. 1998; 98:2334–2351. [PubMed: 9826323]
10. Cowan KN, Heilbut A, Humpl T, Lam C, Ito S, Rabinovitch M. Complete reversal of fatal pulmonary hypertension in rats by a serine elastase inhibitor. Nat Med. 2000; 6:698–702. [PubMed: 10835689]
11. Henkens IR, Mouchaers KT, Vonk-Noordegraaf A, Boonstra A, Swenne CA, Maan AC, Man SC, Twisk JW, van der Wall EE, Schalij MJ, Vliegen HW. Improved ECG detection of presence and severity of right ventricular pressure load validated with cardiac magnetic resonance imaging. Am J Physiol Heart Circ Physiol. 2008; 294:H2150–H2157. [PubMed: 18310513]
12. Hlaing T, Guo D, Zhao X, DiMino T, Greenspon L, Kowey PR, Yan GX. The QT and Tp-e intervals in left and right chest leads: comparison between patients with systemic and pulmonary hypertension. J Electrocardiol. 2005; 38:154–158. [PubMed: 16226092]
13. Henkens IR, Mouchaers KT, Vliegen HW, van der Laarse WJ, Swenne CA, Maan AC, Draisma HH, Schalij I, van der Wall EE, Schalij MJ, Vonk-Noordegraaf A. Early changes in rat hearts with developing pulmonary arterial hypertension can be detected with three-dimensional electrocardiography. Am J Physiol Heart Circ Physiol. 2007; 293:H1300–H1307. [PubMed: 17496210]
14. Lee JK, Nishiyama A, Kambe F, Seo H, Takeuchi S, Kamiya K, Kodama I, Toyama J. Downregulation of voltage-gated K(+) channels in rat heart with right ventricular hypertrophy. Am J Physiol. 1999; 277:H1725–H1731. [PubMed: 10564125]
15. Endo H, Miura M, Hirose M, Takahashi J, Nakano M, Wakayama Y, Sugai Y, Kagaya Y, Watanabe J, Shirato K, Shimokawa H. Reduced inotropic effect of nifekalant in failing hearts in rats. J Pharmacol Exp Ther. 2006; 318:1102–1107. [PubMed: 16738208]
16. Morita N, Sovari AA, Xie Y, Fishbein MC, Mandel WJ, Garfinkel A, Lin SF, Chen PS, Xie LH, Chen F, Qu Z, Weiss JN, Karagueuzian HS. Increased susceptibility of aged hearts to ventricular fibrillation during oxidative stress. Am J Physiol Heart Circ Physiol. 2009; 297:H1594–H1605. [PubMed: 19767530]
17. Saiz J, Ferrero JM Jr, Monserrat M, Ferrero JM, Thakor NV. Influence of electrical coupling on early afterdepolarizations in ventricular myocytes. IEEE Trans Biomed Eng. 1999; 46:138–147. [PubMed: 9932335]
18. Huelsing DJ, Spitzer KW, Pollard AE. Electrotonic suppression of early afterdepolarizations in isolated rabbit Purkinje myocytes. Am J Physiol Heart Circ Physiol. 2000; 279:H250–H259. [PubMed: 10899064]
19. Xie LH, Chen F, Karagueuzian HS, Weiss JN. Oxidative-stress-induced afterdepolarizations and calmodulin kinase II signaling. Circ Res. 2009; 104:79–86. [PubMed: 19038865]
20. Xie Y, Sato D, Garfinkel A, Qu Z, Weiss JN. So little source, so much sink: requirements for afterdepolarizations to propagate in tissue. Biophys J. 2010; 99:1408–1415. [PubMed: 20816052]
21. Sato D, Xie LH, Sovari AA, Tran DX, Morita N, Xie F, Karagueuzian H, Garfinkel A, Weiss JN, Qu Z. Synchronization of chaotic early afterdepolarizations in the genesis of cardiac arrhythmias. Proc Natl Acad Sci U S A. 2009; 106:2983–2988. [PubMed: 19218447]
22. Tomaselli GF, Zipes DP. What causes sudden death in heart failure? Circ Res. 2004; 95:754–763. [PubMed: 15486322]
23. Roepke TK, Kontogeorgis A, Ovanez C, Xu X, Young JB, Purtell K, Goldstein PA, Christini DJ, Peters NS, Akar FG, Gutstein DE, Lerner DJ, Abbott GW. Targeted deletion of kcne2 impairs ventricular repolarization via disruption of I(K, slow1) and I(to, f). FASEB J. 2008; 22:3648–3660. [PubMed: 18603586]

24. Hessel MH, Steendijk P, den Adel B, Schutte CI, van der Laarse. Characterization of right ventricular function after monocrotaline-induced pulmonary hypertension in the intact rat. Am J Physiol Heart Circ Physiol. 2006; 291:H2424–H2430. [PubMed: 16731643]
25. Hessel M, Steendijk P, den Adel B, Schutte C, van der Laarse. Pressure overload-induced right ventricular failure is associated with re-expression of myocardial tenascin-C and elevated plasma tenascin-C levels. Cell Physiol Biochem. 2009; 24:201–210. [PubMed: 19710535]
26. Kogler H, Hartmann O, Leineweber K, Nguyen vP, Schott P, Brodde OE, Hasenfuss G. Mechanical load-dependent regulation of gene expression in monocrotaline-induced right ventricular hypertrophy in the rat. Circ Res. 2003; 93:230–237. [PubMed: 12842921]
27. Lamberts RR, Vaessen RJ, Westerhof N, Stienen GJ. Right ventricular hypertrophy causes impairment of left ventricular diastolic function in the rat. Basic Res Cardiol. 2007; 102:19–27. [PubMed: 16944361]
28. Benoist D, Stones R, Drinkhill M, Bernus O, White E. Arrhythmogenic substrate in hearts of rats with monocrotaline-induced pulmonary hypertension and right ventricular hypertrophy. Am J Physiol Heart Circ Physiol. 2011; 300:H2230–H2237. [PubMed: 21398591]
29. Abbott GW, Sesti F, Splawski I, Buck ME, Lehmann MH, Timothy KW, Keating MT, Goldstein SA. MiRP1 forms IKr potassium channels with HERG and is associated with cardiac arrhythmia. Cell. 1999; 97:175–187. [PubMed: 10219239]
30. Hajjar RJ, Schmidt U, Matsui T, Guerrero JL, Lee KH, Gwathmey JK, Dec GW, Semigran MJ, Rosenzweig A. Modulation of ventricular function through gene transfer in vivo. Proc Natl Acad Sci U S A. 1998; 95:5251–5256. [PubMed: 9560262]
31. Ogawa M, Morita N, Tang L, Karagueuzian HS, Weiss JN, Lin SF, Chen PS. Mechanisms of recurrent ventricular fibrillation in a rabbit model of pacing-induced heart failure. Heart Rhythm. 2009; 6:784–792. [PubMed: 19467505]
32. Morita N, Lee JH, Xie Y, Sovari A, Qu Z, Weiss JN, Karagueuzian HS. Suppression of reentrant and multifocal ventricular fibrillation by the late sodium current blocker ranolazine. J Am Coll Cardiol. 2011; 57:366–375. [PubMed: 21232675]
33. Miura M, Hirose M, Endoh H, Wakayama Y, Sugai Y, Nakano M, Fukuda K, Shindoh C, Shirato K, Shimokawa H. Acceleration of Ca(2+) waves in monocrotaline-induced right ventricular hypertrophy in the rat. Circ J. 2011; 75:1343–1349. [PubMed: 21467666]
34. Campian ME, Verberne HJ, Hardziyenka M, de BK, Selwaness M, van den Hoff MJ, Ruijter JM, van Eck-Smit BL, de Bakker JM, Tan HL. Serial noninvasive assessment of apoptosis during right ventricular disease progression in rats. J Nucl Med. 2009; 50:1371–1377. [PubMed: 19617336]
35. Chan SY, Loscalzo J. Pathogenic mechanisms of pulmonary arterial hypertension. J Mol Cell Cardiol. 2008; 44:14–30. [PubMed: 17950310]
36. van Wolferen SA, Marcus JT, Westerhof N, Spreeuwenberg MD, Marques KM, Bronzwaer JG, Henkens IR, Gan CT, Boonstra A, Postmus PE, Vonk-Noordegraaf A. Right coronary artery flow impairment in patients with pulmonary hypertension. Eur Heart J. 2008; 29:120–127. [PubMed: 18065750]
37. Rich S, Pogoriler J, Husain AN, Toth PT, Gomberg-Maitland M, Archer SL. Long-term effects of epoprostenol on the pulmonary vasculature in idiopathic pulmonary arterial hypertension. Chest. 2010; 138:1234–1239. [PubMed: 21051399]
38. Gomberg-Maitland M, Dufton C, Oudiz RJ, Benza RL. Compelling evidence of long-term outcomes in pulmonary arterial hypertension? A clinical perspective. J Am Coll Cardiol. 2011; 57:1053–1061. [PubMed: 21349396]

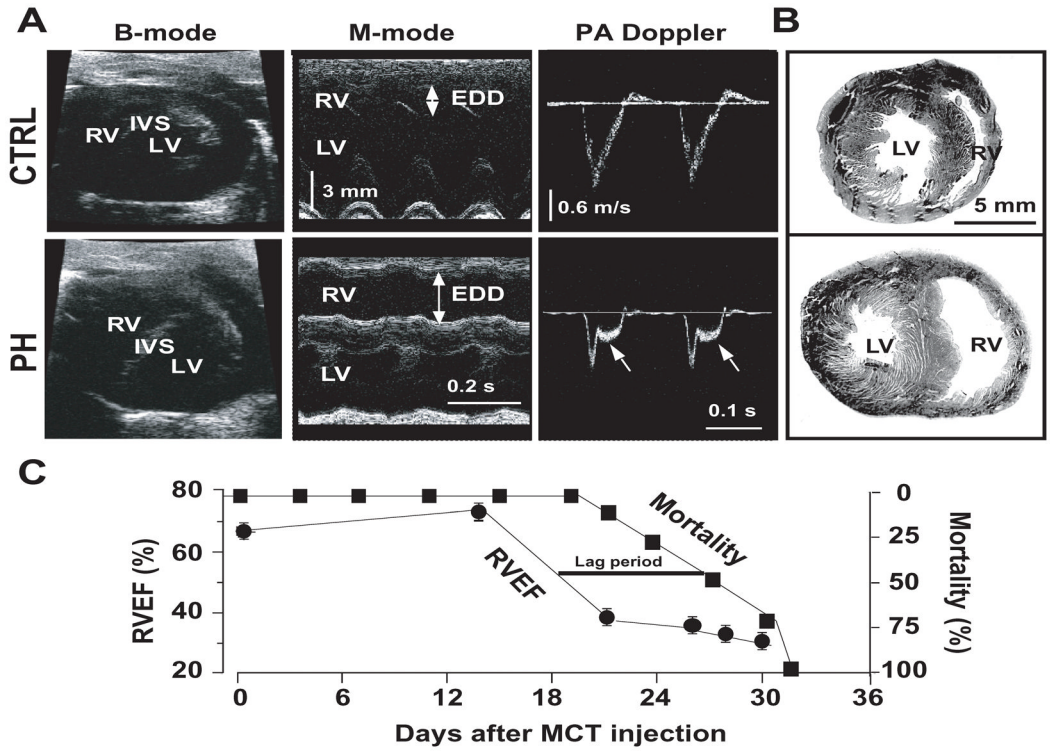

Figure 1.

Cardiac hemodynamics and mortality in rats with PH. Panel **A** shows echocardiographic images of B-mode (left panel), M-mode of heart (middle panel), and pulsed-wave Doppler of pulmonary artery (PA) flow (right panel) where EDD is RV end-diastolic diameter. Arrows in the pulsed-wave Doppler signals show mid-systolic notch in the pulmonary artery flow in PH (n=7 for CTRL and n=6 for PH). Panels **B** shows Hematoxylin-eosin staining of heart cross-sections of CTRL and PH (n=7 for CTRL and n=6 for PH). Panel **C** shows combined time-course of mortality (including sudden unexpected deaths, black squares) and RVEF (black circles) in the PH group (n=24).

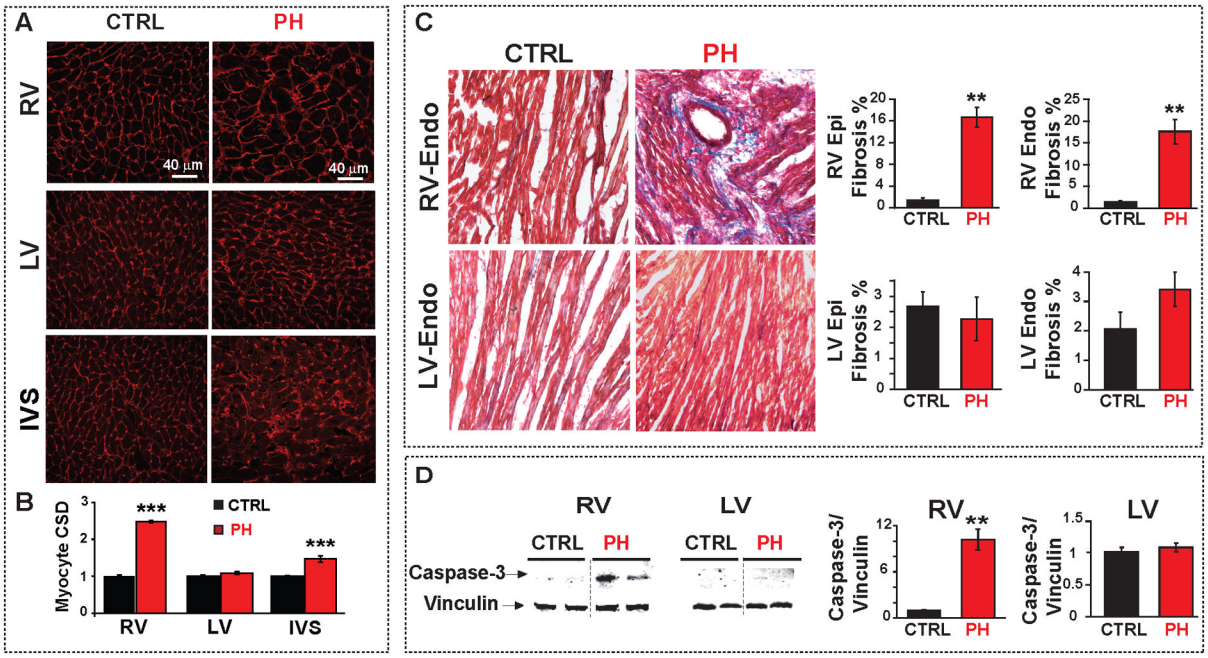

Figure 2.

Cardiac structural changes associated with PH-induced RV-failure**. A.** RV, LV and IVS sections stained with wheat germ agglutinin (red) in CTRL and PH hearts. **B.** Myocyte cross sectional diameter (CSD) of RV, LV and IVS comparing CTRL and PH groups. $^{***}p<0.001$ *vs.* CTRL. (n=3 rats per group and at least 60 cells per group). **C.** Masson trichrome staining of RV and LV-sections in CTRL and PH; blue color indicates fibrosis. Quantification of RV and LV-endocardial and epicardial fibrosis (%) is shown in the right panels. $^{**}p<0.01$ *vs.* CTRL (n=3 rats per group). **D.** Representative immunoblots of RV and LV from CTRL and PH labelled with anti-caspase-3 and anti-vinculin antibodies. Mean levels of cleaved caspase-3 protein normalized to vinculin in CTRL (black bar) and PH (red) are shown at the right ($^{**}p<0.01$ *vs.* CTRL, n=4–7 rats per group)

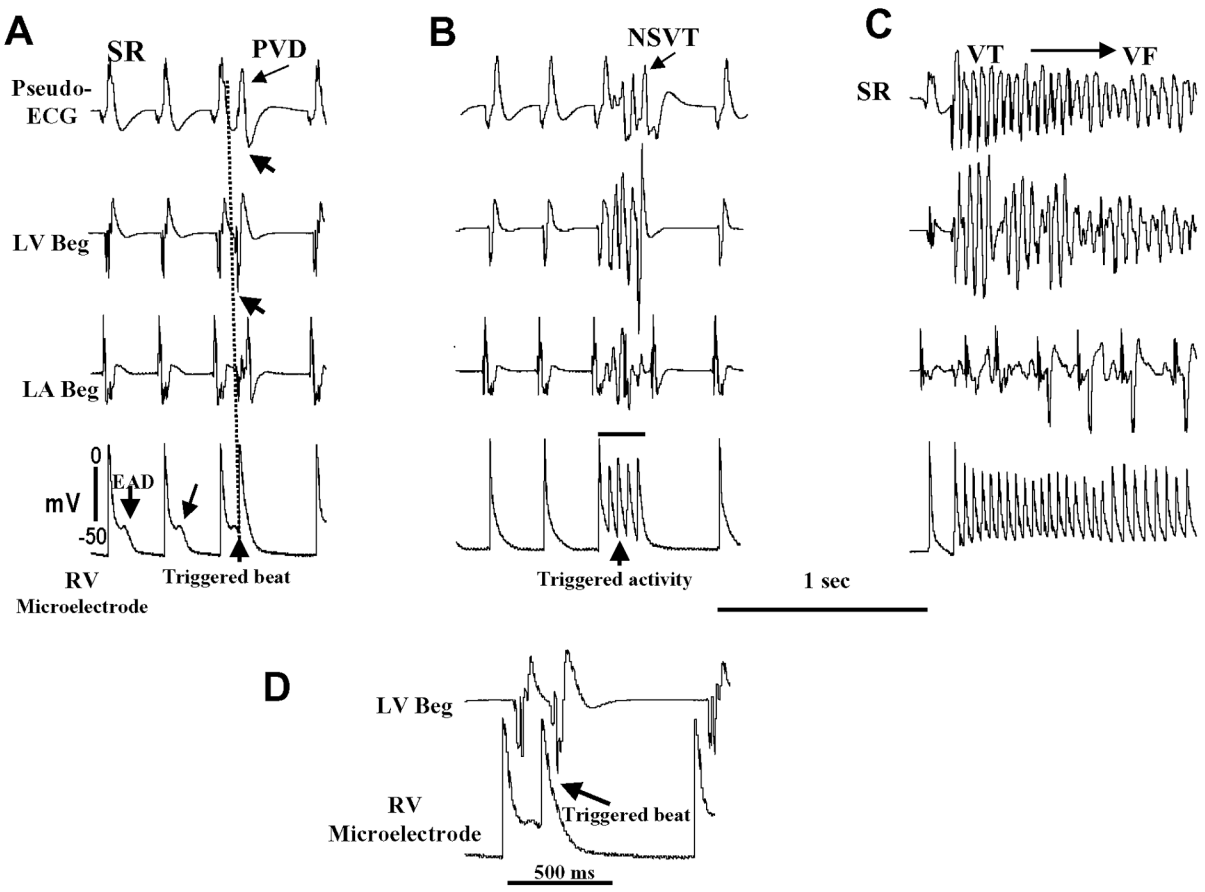

Figure 3.

Emergence of RV epicardial EADs, triggered activity and VF in a heart isolated 29 days after MCT injection. In each panel the recordings from top to bottom are: pseudo-ECG, LV and left atrial bipolar electrograms (LV Beg and LA Beg), and the bottom tracing is single cell microelectrode recording from the RV epicardial base. Panel **A** shows the emergence of an EAD on two consecutive sinus beats (two downward arrows) 28 min after mounting the heart with regular sinus rhythm (SR) at a mean cycle length of 254±18 ms. The EAD associated with the third sinus beat triggers an action potential at a coupling interval of 85 ms (upward arrow) causing a premature ventricular depolarization (PVD) on the pseudo-ECG (arrow). Notice that the emergence of RV epicardial cell EAD is associated with isoelectric interval of the LA Beg, LV Beg and pseudo-ECG recordings indicating absence of electrical activity elsewhere in the heart during the emergence of EADs in the RV. Panel **B** shows recordings 29 min after tissue mounting (1 min after panel A) with the third sinus beat associated with EAD-mediated triggered activity (upward arrow) causing non-sustained ventricular tachycardia (NSVT) (arrow on pseudo-ECG). Panel **C** shows recordings made 2 min after panel B showing EAD-mediated triggered activity to cause VT (~18 beats) which then degenerates to irregular pattern signalling the onset of VF. The VF was then terminated by electrical shock (not shown). Panel **D** shows magnified view of part of the lower 2 recordings of A.

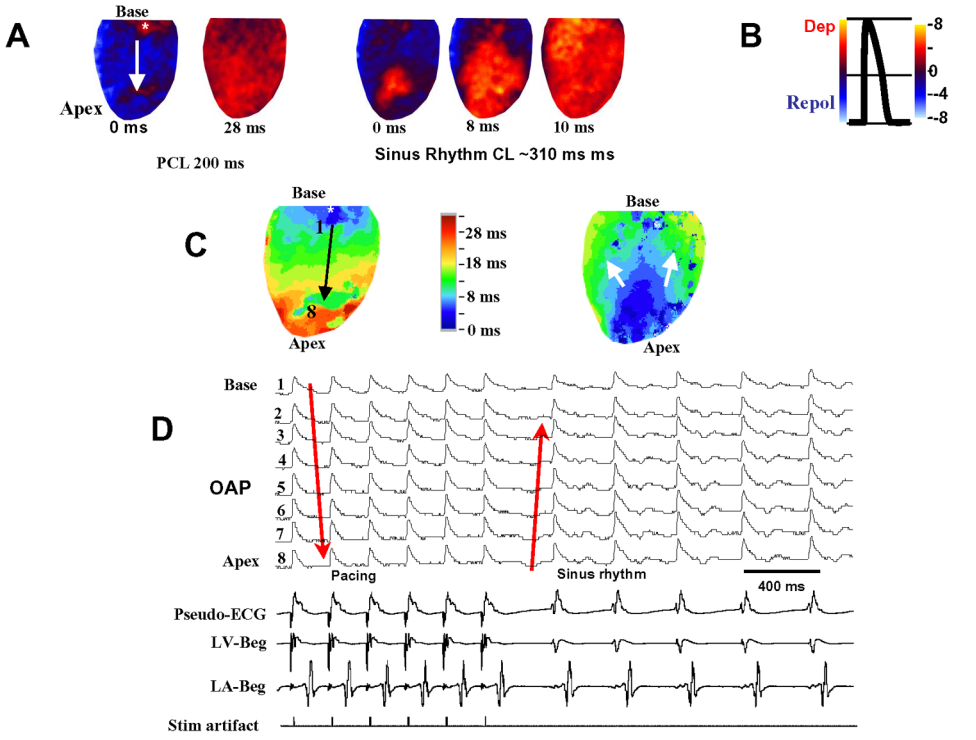

Figure 4.

Optical snap shots, isochronal maps and optical action potentials recorded from the RV epicardium in a heart 29 days after MCT injection. Panel **A** (left) are snapshots during RV pacing from the base at a cycle length of 200 ms and during sinus rhythm (right 3 snap shots) showing total RV epicardial activation within 10 ms. Asterisk at the base of the RV is the pacing site (downward white arrow indicates the direction of propagation) Notice the absence of conduction block during pacing and during sinus rhythm. Time zero is chosen arbitrarily for both pacing and sinus rhythm snapshots. Panel **B** is a schematic drawing of optical action potential (OAP) with blue denoting repolarization and red depolarization. Panel **C** are isochronal maps during pacing (left) and during sinus rhythm (right) of the corresponding snap shots shown in panel A. Arrows in panel C indicate the direction of wavefront propagation. Panel **D** shows simultaneous 8 OAPs recorded from equally spaced sites (1 to 8) identified in panel C (black arrow). Downward pointing red arrow indicates the direction of wavefront propagation during RV pacing from the base and upward pointing red arrow indicates sinus beats. The lower 4 panels in panel D are simultaneous recordings of pseudo-ECG, left ventricular and atrial bipolar electrograms (LV Beg and LA Beg, respectively) and pacing stimulus artefact (bottom tracing). Six paced beats at a cycle length of 200 ms are followed by five beats of sinus origin with a cycle length of ~310 ms.

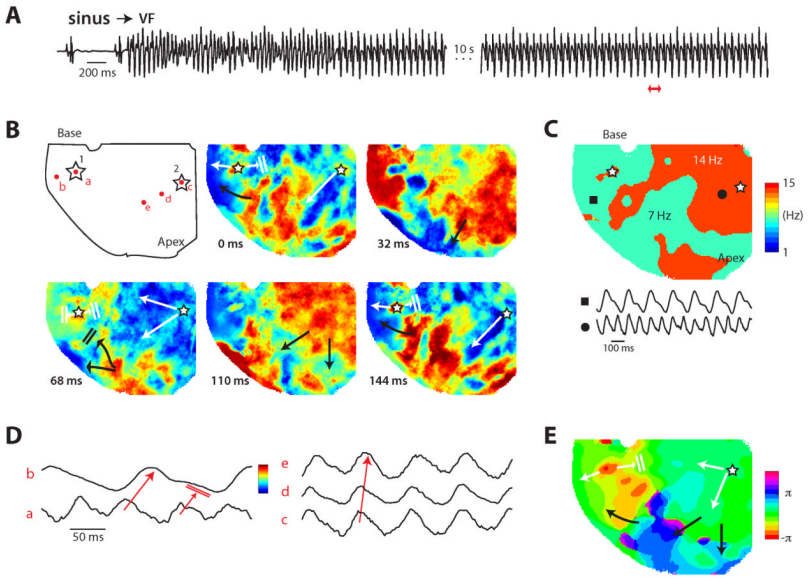

Figure 5.

Optical imaging during spontaneous VF in a heart isolated 29 days after MCT injection. Open stars indicate the two foci, white arrows indicate propagation from foci and black arrows indicate propagation from existing waves. Panel A shows the pseudo-ECG of the onset of the spontaneous VF. The heart was imaged about 15 seconds after onset. The pECG of the imaged period is shown in the second part of the trace, after the 10s break. The red double arrow indicates the period shown in panel B. Panel B shows snap shots of activation during 144 ms of imaged time. The red dots in the first image indicate the locations of the OAPs shown in panel D. See panel D for the color scale of the snap shots in relation to the OAPs. Panel C shows the frequency map with two sample OAPs at the closed circle and square. Panel D shows OAPs highlighting the propagation from the foci 1 (OAPs a and b) and 2 (OAPs c, d and e) indicated in panel B. Panel E shows the phase (π) map of the 7 Hz activity. The activity continued and arrived at the apex beyond the end of the period (i.e., the foci had already fired the second time), so this late activity near the apex was unwrapped to the 2π complement for clarity.

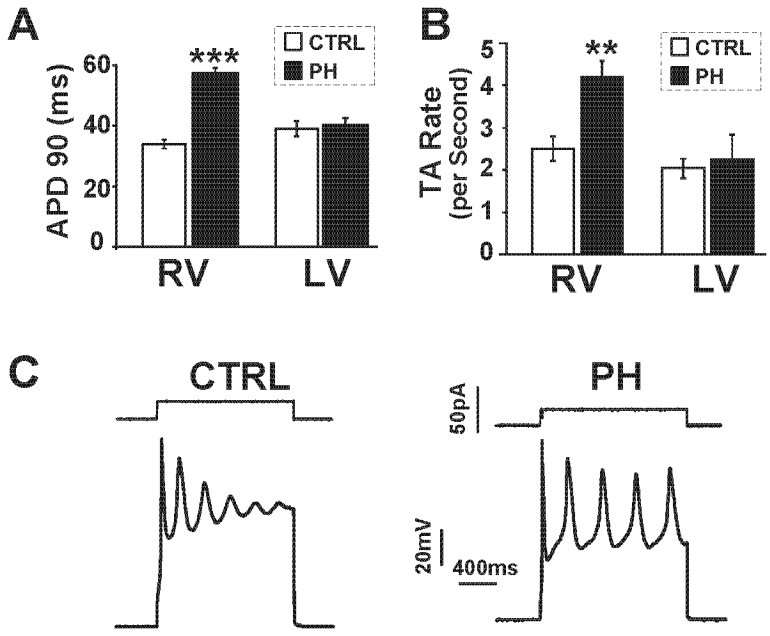

Figure 6.

APD prolongation and triggered activity in isolated RV cardiomyocytes. **A**. Bar graph showing mean action potential duration at 90% repolarization (APD90) in RV and LV cardiomyocytes from CTRL (white bar) and PH (black bar) ($^{***}p<0.001$ *vs.* CTRL, n=16–20 cells for RV and n=5 cells for LV from 5 rats/group). **B.** Bar graphs showing rate of depolarizing current-induced triggered activity (TA) (per second) in RV and LV cardiomyocytes from CTRL (white bar) and PH (black bar) ($^{**}p<0.01$ *vs.* CTRL n=5 cells from 5 rats/group). **C.** Depolarizing current-induced triggered activity in isolated RV-cardiomyocytes from CTRL and PH.

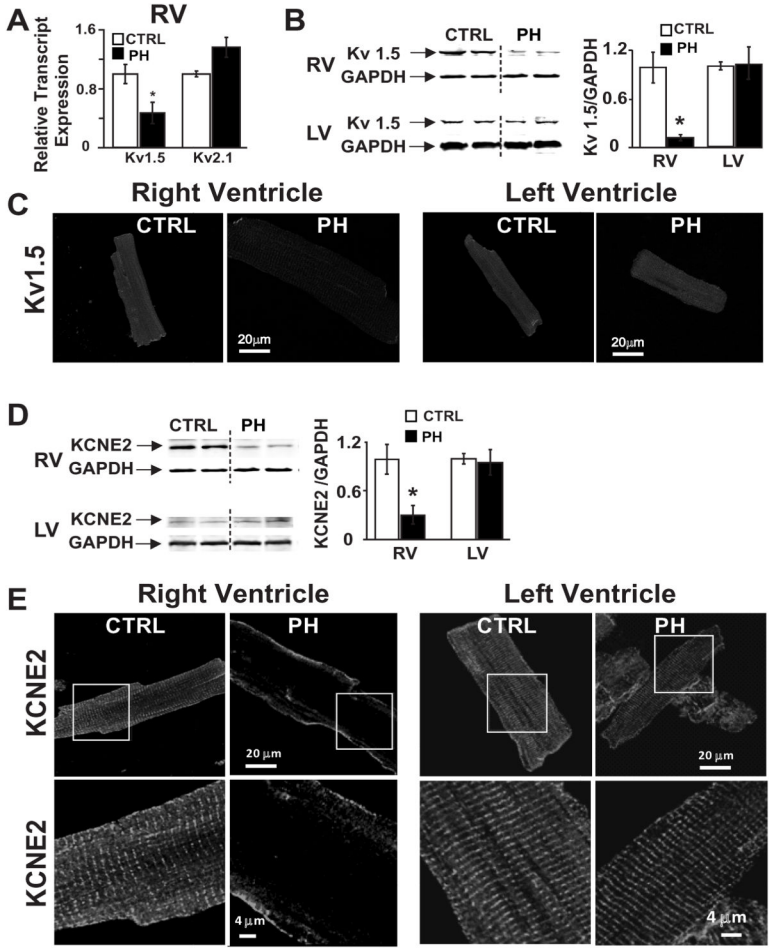

Figure 7.

Alteration of Kv1.5 and KCNE2 expression in PH. **A.** Relative transcript levels of Kv1.5 and Kv 2.1 in CTRL (white bar), and PH (black bar) normalized to CTRL are shown ($^{*}p<0.05$ *vs.* CTRL, n=3–4/group). **B.** Representative immunoblots of RV and LV (left panel) from CTRL and PH labelled with anti-Kv1.5 and anti-GAPDH antibodies. Mean protein levels of Kv1.5 protein (right panel) normalized to GAPDH in CTRL (white bar) and PH (black) are shown ($^{*}p<0.05$ *vs.* CTRL, n=3–4/group). **C.** Immunofluorescence images of isolated RV and LV cardiomyocytes stained for Kv1.5 are shown from CTRL and PH. **D.** Representative immunoblots of RV and LV (left panel) from CTRL and PH labelled with anti-KCNE2 and anti-GAPDH antibodies. Mean protein levels of KCNE2 normalized to GAPDH (right panel) in CTRL (white bar) and PH (black) are shown. ($^{*}p<0.05$ *vs.* CTRL, n=3–4/group). **E.** Immunofluorescence images of isolated cardiomyocytes stained for KCNE2 are shown from CTRL and PH of RV (left panel) and LV (right panel).

Table 1

Cardiac functional and structural characteristics of rats with pulmonary hypertension.

	CTRL (n=6–7)	PH (n=6–7)
RVPSP (mm Hg)	**31±1**	**72±1.5*****
LVDP (mm Hg)	**104±3.5**	**100±3**
RV EF (%)	**65±1**	**33±3*****
LV EF (%)	**71±1**	**67±2.6**
RV/(LV+IVS)	**0.24±0.02**	**0.66±0.08*****
LV/Body weight (mg/g)	**1.71±0.20**	**1.58±0.06**
IVS/Body weight (mg/g)	**0.84±0.06**	**0.90±0.07**

CTRL is control, PH is pulmonary hypertension, RV is right ventricle, LV is left ventricle, IVS is interventricular septum, RVPSP is right ventricular peak systolic pressure, LVDP is left ventricular developed pressure, RVEF is right ventricular ejection fraction, LVEF is left ventricular ejection fraction. The parameters were measured 4 weeks after either PBS injection in CTRL group or MCT injection in the PH group. Values are mean±SEM,

*** $p<0.001$ vs. CTRL.